Heliyon 10 (2024) e37219

Contents lists available at ScienceDirect

Heliyon

journal homepage: www.cell.com/heliyon

Research article

Dual role of targeting NAE1 in nasopharyngeal carcinoma: Antitumor effects yet inducing radiotherapy resistance

Qinsong Liu, Lu Xin, Xiaoning Ma, Yong Yuan *

Department of Otolaryngology, Qingdao Municipal Hospital, Qingdao, Shandong, China

ARTICLE INFO

Keywords:
NAE1
MLN4924
Nasopharyngeal carcinoma
Radiosensitivity
Cell cycle

ABSTRACT

Background and objectives: The inhibitor MLN4924 of Neural Precursor Cell-Expressed Developmentally Down-Regulated 8 (NEDD8) Activating Enzyme 1 (NAE1) has been found to suppress the growth of nasopharyngeal carcinoma (NPC). However, its effect on NPC's radiotherapy sensitivity remains unclear.

Methods: By integrating single-cell RNA sequencing and bulk RNA sequencing, we predict the impact of NAE1 on the cell cycle, cell death, and its relationship with radiotherapy sensitivity and prognosis in NPC. The effect of inhibiting NAE1 on NPC cell behavior and radiation sensitivity is explored through MLN4924 intervention in vitro and in vivo. We construct a prognosis prediction model based on NAE1 using machine learning methods and validate the efficacy of NAE1 and the model in clinical cohorts.

Results: NPC patients with high NAE1 expression have better prognosis and higher expression in the radiotherapy-sensitive group. Inhibiting NAE1 with MLN4924 causes cell cycle arrest in NPC cells, preventing them from entering the G2/M phase, thereby inhibiting proliferation but not affecting migration and metastasis. However, in vitro and in vivo experiments demonstrate that inhibiting NAE1 with MLN4924 leads to increased resistance of NPC to radiation.

Conclusions: Targeting NAE1 for NPC treatment may have dual effects, inhibiting NPC proliferation while also increasing radiation resistance.

1. Introduction

Nasopharyngeal carcinoma (NPC) is a prevalent malignancy in southern China, ranking highest among head and neck cancers. The most common histological types of NPC are poorly differentiated squamous cell carcinoma and undifferentiated carcinoma, which are notably sensitive to radiation. Consequently, radiotherapy is one of the primary treatment modalities for NPC [1]. High-energy radiation is employed to destroy cancer cells and can be administered through external beam radiotherapy or brachytherapy. Radiotherapy is typically used for both early and advanced stages of NPC, and often in combination with other therapeutic approaches [2]. However, prolonged exposure of tumor cells to radiation can lead to abnormal expression of certain genes and proteins, resulting in reduced radiosensitivity and the development of radioresistance [3].

Pevonedistat (MLN4924) is a novel small-molecule inhibitor that selectively inhibits Neural precursor cell-Expressed Developmentally down-regulated 8 (NEDD8) Activating Enzyme 1 (NAE1) [4]. NAE1 is a key molecule in the NEDDylation pathway; inhibition of this pathway leads to the accumulation of various substrates of Cullin-Ring Ligases E3 (CRL), including Chromatin Licensing and

* Corresponding author. NO. 1, Shibei District, Jiaozhou Road, Qingdao, Shandong, 266011, China.
E-mail address: entyy2083@163.com (Y. Yuan).

https://doi.org/10.1016/j.heliyon.2024.e37219
Received 29 June 2024; Received in revised form 21 August 2024; Accepted 29 August 2024
Available online 30 August 2024

DNA Replication Factor 1 (CDT1), Cyclin Dependent Kinase (CDK) inhibitors p21 and p27, and WEE1 G2 Checkpoint Kinase (Wee1) [5]. This accumulation results in cell cycle arrest at the G2/M phase, leading to apoptosis and senescence [6]. MLN4924 effectively inhibits tumor cell growth by inducing three common types of cell death—apoptosis, autophagy, and senescence [7], and has also been shown to impact DNA damage repair [4]. MLN4924 is currently in phase II clinical trials for both hematologic malignancies [8,9] and solid tumors [10,11].

Although these drugs exert antitumor effects through a complex array of mechanisms, they may also induce unexpected side effects, such as altered radiosensitivity. Current understanding suggests that genes involved in DNA repair, cell proliferation and cycle regulation, and apoptosis/anti-apoptosis are closely associated with radioresistance in NPC [12]. There is a close relationship between the cell cycle and radiosensitivity. Radiotherapy works by damaging the DNA of cancer cells to prevent their division and growth [13]. Because different phases of the cell cycle exhibit varying sensitivities to radiation, the state of the cell cycle can influence the efficacy of radiotherapy. Cells in the G2 and M phases are relatively more sensitive as they are preparing for or undergoing mitosis and have less efficient DNA repair capabilities [14]. Conversely, cells in the G0 and G1 phases are more resistant to radiation, being in a dormant state or preparing to enter the S phase, where DNA replication activity is lower, making them less affected by radiation [14].

Studies have demonstrated that inhibiting the NEDDylation pathway can suppress NPC proliferation [15]. However, considering that nearly all NPC patients require radiotherapy, the impact of NAE1 inhibitors on the radiosensitivity of NPC warrants further investigation.

2. Material and methods

2.1. Clinical sample collection

Human tissue samples used and collected in this study were conducted in accordance with the guidelines of the International Organization of Medical Sciences and the World Health Organization. Ethical approval was obtained from the Ethics Committee of Qingdao Municipal Hospital (Approval No: 2024-KY-032). Informed consent was obtained from all patients participating in the study. All patients were staged according to the 8th edition of the AJCC (American Joint Committee on Cancer) TNM staging system, and the baseline information of the 46 patients included in the prognosis study was collected (Table 1). The patients' tissue samples were collected from forceps biopsy specimens obtained at the Department of Otolaryngology-Head and Neck Surgery, Qingdao Municipal Hospital.

2.2. Transcriptomic sequencing analysis

Single-cell RNA sequencing (scRNA-seq) data were sourced from the GEO database, specifically from datasets GSE150825 and

Table 1
Characteristics of 46 patients with NPC.

Patient characteristic	No. of patients (n = 46)
Age	
Median	59 (range 37–69)
Sex	
Male	26
Female	20
Treatment	
Radiotherapy	21
Radiotherapy + Chemotherapy	25
Others	0
T	
T1	3
T2	10
T3	31
T4	2
N	
N0	2
N1	29
N2	12
N3	3
M	
Mx	2
M0	43
M1	1
EBV DNA	
Positive	44
Negative	2
Pathological type	
Keratinizing	5
Non-keratinizing	41

GSE150430. Primary NPC samples and nasopharyngeal lymphatic hyperplasia (NLH) samples were selected for analysis. Quality control was performed using the Seurat package with the following criteria: 1) cells with ≥200 features and <5000 features were retained; 2) cells with mitochondrial gene reads constituting <20 % of the transcriptome were retained; 3) cells with <8000 counts were retained. Data normalization was conducted using SCTransform. Doublets were removed using the DoubletFinder tool. Subsequent analyses, including principal component analysis, unsupervised clustering, and cell cluster annotation, were performed using the Seurat package. Cell cycle analysis was conducted using the CellCycleScoring function in Seurat. Gene Set Enrichment Analysis (GSEA) was carried out using the clusterProfiler package. Copy number variation analysis was performed using the copykat package. Weighted Gene Co-Expression Network Analysis (WGCNA) was carried out using the WGCNA package.

Bulk RNA-seq and transcriptome microarray data were obtained from the GEO database, specifically from datasets GSE32389 and GSE102349. The GSE32389 dataset includes a comparison design between radiotherapy-sensitive and resistant groups. The GSE102349 dataset contains progression-free survival (PFS) information of patients. Raw expression matrices were converted to transcripts per million (TPM), and data normalization was performed using the limma package. GSEA was conducted using the clusterProfiler package. Survival analysis was performed using the survival package. Heatmaps were generated using the pheatmap package.

2.3. Cell culture and treatment

The tumor cell lines HNE1, HNE2, FTC-133, Hep G2, U251 and MCF7 were purchased from Abiowell Biotechnology Co., Ltd. (Changsha, China) and were authenticated for species origin using Short Tandem Repeat (STR) analysis. These cells were cultured in DMEM high glucose medium (glucose <4500 mg/L) supplemented with 10 % heat-inactivated fetal bovine serum and penicillin-streptomycin. For cell cycle analysis and drug toxicity experiments, cells were treated with MLN4924 at a final concentration of 0.3 μM dissolved in DMSO for 24 h [7]. Cell cycle detection and CCK8 assays were then performed. For radiotherapy sensitivity experiments, cells were treated with MLN4924 at a final concentration of 0.3 μM dissolved in DMSO for 24 h, followed by exposure to single doses of X-ray irradiation at 2, 4, 6, 8, and 10 Gy. Control cells for MLN4924 treatment were treated with DMSO. We also designed experiments with concentration gradients of 0.1, 0.3, 1, 5, and 10 μM to determine the drug's effects at different concentrations.

2.4. Flow cytometry for cell cycle analysis

Control or treated tumor cells in normal growth conditions were counted, and 2 × 10^5 cells per group were plated. After cell attachment, the regular culture medium was replaced with serum-free DMEM and cultured for 20 h to synchronize all cells to the same cell cycle phase. Post-synchronization, the medium was replaced with DMEM containing 10 % fetal bovine serum (FBS), and cells were cultured for an additional 24 h. Cells were then trypsinized using EDTA-free trypsin, collected, and centrifuged for washing. Cells were resuspended in precooled 70 % ethanol and fixed overnight at 4 °C. Ethanol was removed, and cells were washed and resuspended in PBS. RNase was added to a final concentration of 100 μg/mL, and cells were digested in a 37 °C water bath for 30 min. Propidium iodide (PI) was added to a final concentration of 50 μg/mL, and cells were incubated in the dark for 15 min before flow cytometry analysis.

2.5. Invasion assay

Matrigel (Beyotime) was dissolved overnight at 4 °C. It was diluted 1:1 with serum-free precooled DMEM. 100 μL of the diluted gel was added to the upper chamber of a 24-well transwell insert. The insert was incubated at 37 °C for 5 h. The gel was gently washed with serum-free DMEM. Cells were resuspended and counted to approximately 5 × 10^5 cells/mL, and 200 μL of the cell suspension was added to the upper chamber. The lower chamber of the transwell was filled with 800 μL of DMEM complete medium containing 20 % FBS. Cells were cultured for 24 h in an incubator. Non-invading cells in the upper chamber were removed with a cotton swab. Cells were fixed with 4 % paraformaldehyde at room temperature for 30 min and stained with crystal violet at room temperature for 30 min. After appropriate air drying, the invading cells were photographed and counted.

2.6. Wound healing assay

Approximately 5 × 10^5 cells were added to each well of a 6-well plate and cultured in complete DMEM medium containing 10 % FBS until confluence was above 90 %. A line was scratched with a 10 μL pipette tip at intervals of 0.5 cm. Cells were washed 3 times with PBS to remove the dislodged cells and replaced with serum-free DMEM. Cells were cultured at 37 °C with 5 % CO2, and images were captured at 0, 6, 12, 24, and 48 h for analysis.

2.7. Colony formation assay

Cells in the logarithmic growth phase were trypsinized and resuspended in complete DMEM medium containing 10 % FBS to create a cell suspension. 500 cells per well from each experimental group were seeded into the wells of a 6-well plate. Cells were cultured for 14 days or until most individual clones contained more than 50 cells. Medium was changed every 3 days, and cell status was observed under a microscope. Cells were fixed with 4 % paraformaldehyde for 30 min per well and stained with 1 mL crystal violet dye for 20

min per well. After PBS washing and air drying, images were taken.

2.8. CCK8 assay

The culture medium was aspirated from the 96-well plate cell culture system, and cells were washed 3 times with PBS. 90 μL of serum-free DMEM was added to each well, followed by 10 μL of CCK-8 solution per well. The 96-well plate was incubated for 2 h at 37 °C in a cell culture incubator with 5 % CO2. Optical density (OD) at 450 nm was measured using a microplate reader to determine cell viability in each well.

2.9. Animal experiments

Animal experiments were approved by the Ethics Committee of Qingdao Municipal Hospital (Approval No.: 2024-KY-032). HNE1 cells in the logarithmic growth phase were digested, centrifuged, and resuspended in PBS at a concentration of 2 × 10^7 cells/mL. A 100 μL cell suspension was injected subcutaneously into the right axilla of 6-week-old BALB/c-nu nude mice. Mice received tail vein injections of a low dose (1 mg/kg) of MLN4924 on days 1, 3, 5, and 7. The control group was injected with DMSO at the same concentration. On day 7, when tumor diameters reached approximately 100 mm^3 in each group, a total irradiation dose of 12 Gy (2 Gy/day for 6 days) was administered. Tumor volume was calculated using the formula: Volume = 0.5 × length × width [2].

2.10. q-PCR

Tissue blocks were placed into grinding bowls, and a small amount of liquid nitrogen was added for rapid grinding. The collected tissue debris was placed in 1.5 mL EP tubes, washed with PBS, and 1 mL of Trizol (Invitrogen) was added. The mixture was allowed to stand at room temperature for 5 min. To each tube, 200 μL of chloroform was added, and the tube was inverted and shaken for 30 s until the mixture appeared milky white. It was then left standing on ice for 5 min. The upper colorless liquid was aspirated from the grinding tube and transferred to a new 1.5 mL EP tube, with each tube containing approximately 400–500 μL. An equal amount of isopropanol was added, mixed thoroughly, and left standing on ice for 10 min. Under conditions of 4 °C and 12,000 rpm, centrifugation was performed for 10 min, resulting in a white precipitate at the bottom of the tube. The precipitate was washed twice with 75 % ethanol. Placed on ice at an incline to air dry, 10 μL of RNase-free water was added to dissolve RNA. The concentration and purity were measured at wavelengths of 260 nm/280 nm using a spectrophotometer. The SweScript RT II First Strand cDNA Synthesis Kit (Servicebio) was used to remove genomic DNA and reverse transcribe mRNA into cDNA. RT-qPCR was performed using Fast SYBR Green qPCR Master Mix (Servicebio) on the machine. The reaction program was set as follows: pre-denaturation at 95 °C for 30 s, 1 cycle; denaturation at 95 °C for 10 s, 40 cycles; annealing/extension at 60 °C for 30 s, 40 cycles. Primers were synthesized by Sangon Biotech Co., Ltd. (Shanghai, China). The forward and reverse primers for the specified genes are designed as follows: TPI1 (Forward Primer: 5′-TCCTTGTGGGTGGTGCTTCC-3’; Reverse Primer: 5′-TGGGCTTCTGGGCTGCTTAG-3′); PUM1 (Forward Primer: 5′-GAACCAGCAGGGACAGCAAAC-3’; Reverse Primer: 5′-GTAAGCAGCAGGAGCCAACAC-3′); GAPDH (Forward Primer: 5′-ACACCCACTCCTCCACCTTTG-3’; Reverse Primer: 5′-TCCACCACCCTGTTGCTGTAG-3′); GPX1 (Forward Primer: 5′-AGAATGTGGCGTCCCTCTGAG-3’; Reverse Primer: 5′-CGTTCTTGGCGTTCTCCTGATG-3′); ZZZ3 (Forward Primer: 5′-AGTCAGCGTCTGCCTTACTATCC-3’; Reverse Primer: 5′-CACACCTCCACTCCTAACACCTAG-3′); MECOM (Forward Primer: 5′-CAGTCAGTGCCCTCTATGTTCAAC-3’; Reverse Primer: 5′-GGTTCTCAAGTGCCGTGTTAGG-3′); LINC00869 (Forward Primer: 5′-CATCACCAATCCATCGCCAGAAG-3’; Reverse Primer: 5′-GAGGAGGAGGAGGAGGAGGAG-3′); CDH1 (Forward Primer: 5′-CGAGAGCTACACGTTCACGG-3’; Reverse Primer: 5′- GGGTGTCGAGGGAAAAATAGG-3′); OCLN (Forward Primer: 5′- ACAAGCGGTTTTATCCAGAGTC-3’; Reverse Primer: 5′- GTCATCCACAGGCGAAGTTAAT-3′); CDH2 (Forward Primer: 5′-TCAGGCGTCTGTAGAGGCTT-3’; Reverse Primer: 5′- ATGCACATCCTTCGATAAGACTG-3′); VIM (Forward Primer: 5′- GACGCCATCAACACCGAGTT-3’; Reverse Primer: 5′- CTTTGTCGTTGGTTAGCTGGT-3′); MMP2 (Forward Primer: 5′- TACAGGATCATTGGCTACACACC-3’; Reverse Primer: 5′- GGTCACATCGCTCCAGACT-3′); ITGB1 (Forward Primer: 5′- CCTACTTCTGCACGATGTGATG-3’; Reverse Primer: 5′- CCTTTGCTACGGTTGGTTACATT-3′).

2.11. Immunohistochemistry

Freshly excised tissue samples were fixed with 10 % paraformaldehyde for over 24 h, dehydrated, and transparentized. After embedding in paraffin for preservation, pathological sections were prepared. Before staining, sections were dewaxed and subjected to antigen retrieval using Tris-EDTA antigen retrieval solution (Servicebio). Sections were blocked with 20 % BSA at room temperature for 30 min. After removing the blocking solution, sections were incubated with diluted anti-NAE1 primary antibody (proteintech, Cat No. 14863-1-AP) overnight at 4 °C. After removing the primary antibody dilution, sections were incubated with horseradish peroxidase-labeled secondary antibody. After removing the secondary antibody, DAB chromogenic solution was added, and the sections were stained at room temperature for 30 min. The staining time was controlled under a microscope, and counterstaining was performed with hematoxylin. After sealing, sections were scanned using a white light scanner. Nuclei stained with hematoxylin appeared blue, and positive expression revealed by DAB was brownish-yellow. The criteria for determination were: positive cell percentage ≥ 70 % (++); positive cell percentage ≥ 20 % (+); positive cell percentage <5 % (±).

2.12. Statistical analysis

For independent samples with normal distribution and homogeneity of variances, the *t*-test was employed. For non-normally distributed data, the Wilcoxon rank-sum test was used. Paired samples were analyzed using the paired *t*-test. When comparing multiple samples, one-way analysis of variance (ANOVA) was applied, followed by pairwise comparisons using the SNK-Q test. Statistical significance was defined as $p < 0.05$ (*), $p < 0.01$ (**), $p < 0.001$ (***), and $p < 0.0001$ (****).

3. Results

3.1. NAE1 correlates with prognosis, radiation sensitivity, and cell cycle progression in NPC

Patients with high NAE1 expression exhibited significantly better PFS compared to those with low NAE1 expression (Fig. 1A). NAE1 expression was also significantly elevated in radiotherapy-sensitive samples (Fig. 1B). Moreover, genes associated with the G2 and M phases were prominently expressed in the radiotherapy-sensitive samples (Fig. 1C). In the scRNA-seq data, we first used CopyKAT to infer malignant cells (Figs. S1A–C). In the UMAP plot, cells located in the lower left corner are inferred to be non-malignant (Fig. S1B); these cells are predominantly in the G1 phase (Fig. 1D) and do not express NAE1 (Fig. 1E). In contrast, malignant cells in the upper right region (Fig. S1B), aside from the quiescent G1 phase cells, are largely in the proliferative G2/M phase and exhibit high NAE1 expression (Fig. 1D–E). Following treatment of HNE1 and HNE2 cells with the selective NAE1 inhibitor MLN4924, the proportion of cells in the G2 phase significantly decreased (Fig. 1F–G). Aside from the G2 phase, there was also a slight decrease in the S phase, while the number of G1 phase cells increased (Fig. 1F–G). In our pan-cancer analysis, we found that the expression of the NAE1 gene is highly positively correlated with the E2F signaling pathway, the MYC signaling pathway, and especially with the G2 checkpoint gene set, suggesting that its primary function may be to alter the cell cycle (Fig. S2).

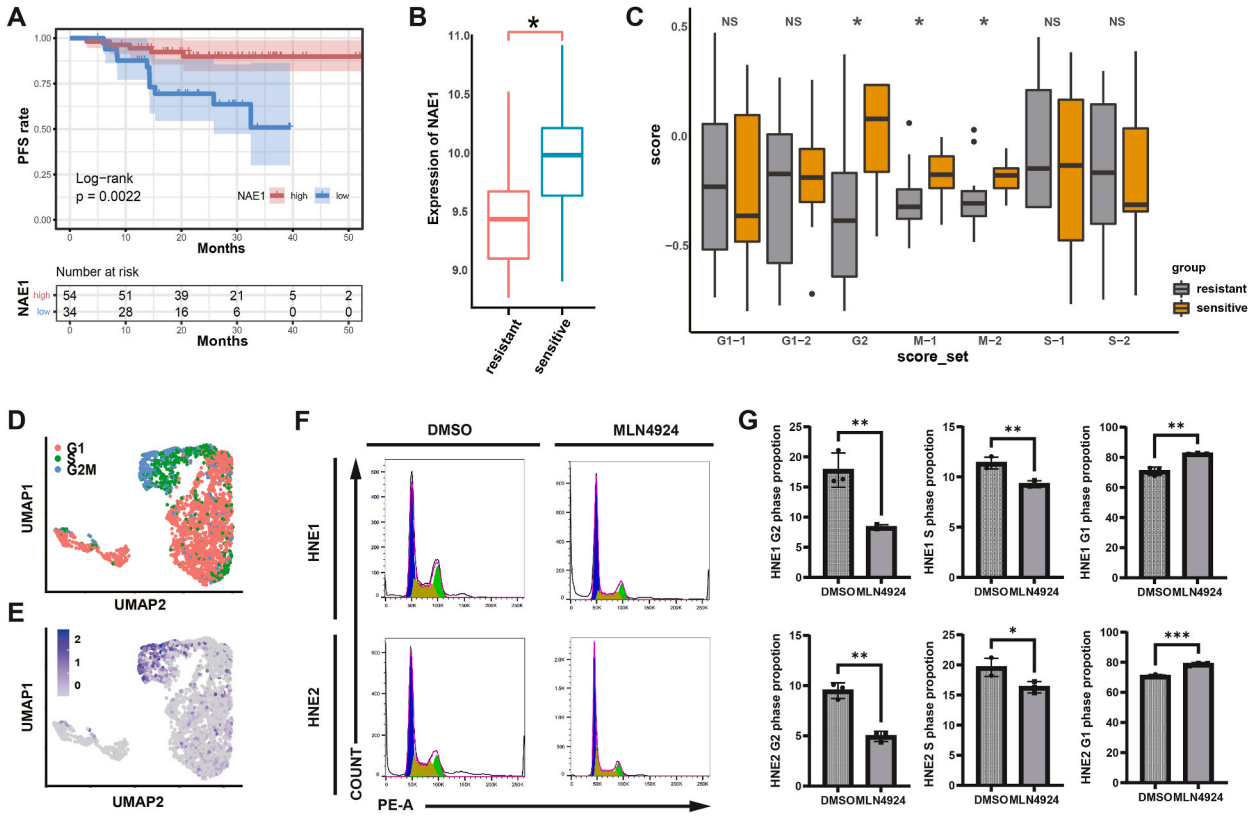

Fig. 1. NAE1's correlation with prognosis, radiotherapy sensitivity, and cell cycle progression in NPC. (A) Kaplan-Meier curves showing progression-free survival rates for high and low NAE1 expression groups, with log-rank test calculations (p-value). (B) Box plot displaying NAE1 expression levels in radiotherapy-resistant and sensitive groups, significance: *P < 0.05. (C) Box plot showing scores of cell cycle gene sets in radiotherapy-resistant and sensitive groups, significance: *P < 0.05. (D) UMAP plot illustrating inferred cell cycle states in nasopharyngeal cancer. (E) UMAP plot showing NAE1 expression levels in nasopharyngeal cancer cells. (F) Histogram depicting PE dye uptake levels in HNE1 and HNE2 cells across different treatments; blue represents G1 phase cells, brown represents S phase cells, and green represents G2 phase cells. (G) Bar graph showing the proportion of G1, S or G2 phase cells in different treatment groups, significance: **P < 0.01.

3.2. MLN4924 selectively inhibits NAE1 to suppress NPC cell proliferation but does not affect invasion or metastasis

After 7 days of 0.3 μM MLN4924 treatment, the number of single-cell colonies and total colony numbers of HNE1 and HNE2 decreased (Fig. 2C–F). We also compared the effects of different concentrations of MLN4924 on the cell viability of HNE1 and HNE2 (Figs. S3A–B). The CCK8 assay results showed that there was almost no inhibitory effect on cell viability at a concentration of 0.1 μM. Starting from 0.3 μM, the inhibitory effect increased with higher doses. In invasion assays, treatment with MLN4924 did not result in significant changes in the average number of invasive cells per field for HNE1 and HNE2 (Fig. 2A–B). Scratch assays indicated no significant changes in healing rates at 0 h, 12 h, 24 h, and 48 h post-treatment with MLN4924 for both HNE1 and HNE2 (Fig. 2G–H). To explain this phenomenon, we compared the mRNA expression of genes related to metastasis and invasion in HNE1 before and after MLN4924 treatment and found no significant differences (Fig. S4).

3.3. MLN4924 selectively inhibits NAE1-mediated radioresistance in NPC cells

Following irradiation with 0, 2, 4, 6, 8, and 10 Gy X-rays and subsequent 48-h culture, cell viability was assessed using the CCK8 assay (Fig. 3A). The results showed that cell viability was slightly reduced in non-irradiated cells treated with MLN4924. At a radiation dose of 10 Gy, the viability of MLN4924-treated cells was higher than that of the control group for both cell lines. After a 10 Gy X-ray exposure and 14 days of culture, the number of cell colonies formed in the MLN4924-treated group was significantly higher than that in the control group (Fig. 3B–C). In vivo, MLN4924 injection did not alter tumor size in nude mice that did not receive radiation treatment (Fig. 3D–F). In irradiated mice, tumors in the MLN4924 injection group were larger than those in the control group (Fig. 3D–F). In addition to NPC, we analyzed the relationship between NAE1 expression and prognosis in various other types of tumors using the TCGA database and found that the relationship between NAE1 and prognosis is heterogeneous across different tumors (Figs. S5A–B). Additionally, we treated several other tumor cell lines besides NPC with MLN4924, including follicular thyroid carcinoma (FTC-133), hepatocellular carcinoma (Hep G2), glioma (U251), and breast cancer (MCF7). The results showed that a low dose of MLN4924 (0.3 μM) had a significant cytotoxic effect only on Hep G2 and MCF7 cells, while a high dose (5 μM) exhibited a significant

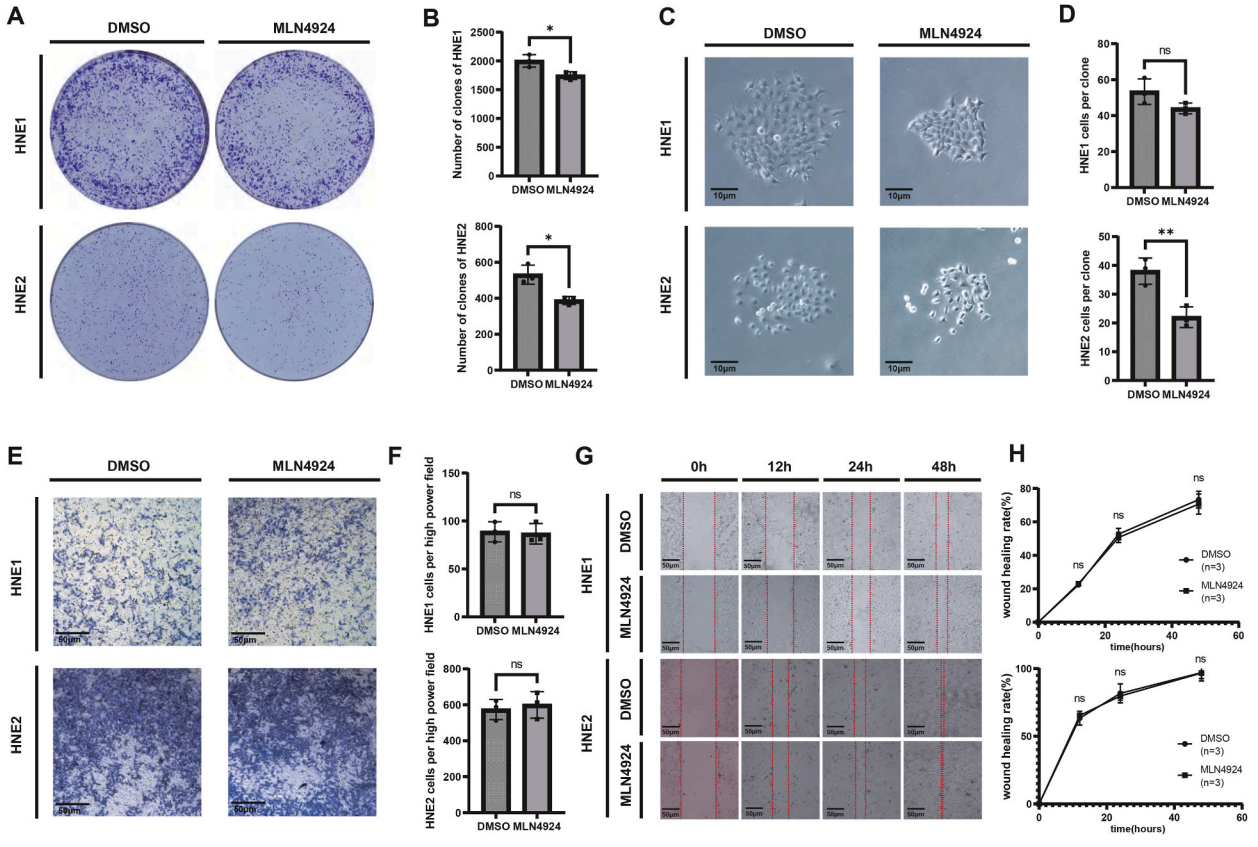

Fig. 2. Cellular behavioral changes in NPC cells following MLN4924 treatment. (A) Overall image of clone formation assays in different treatment groups. (B) Statistical analysis of clone numbers in clone formation assays, *P < 0.05. (C) Single clone formation in different treatment groups. (D) Statistical analysis of single clone numbers in clone formation assays, significance: **P < 0.01, $^{ns}P \geq 0.05$. (E) Cells migrated into the lower chamber in Transwell assays under different treatments. (F) Statistical analysis of Transwell assay results, significance: $^{ns}P \geq 0.05$. (G) Scratch assay results in different treatment groups. (H) Statistical analysis of wound healing rates at different time points in scratch assays, significance: $^{ns}P \geq 0.05$.

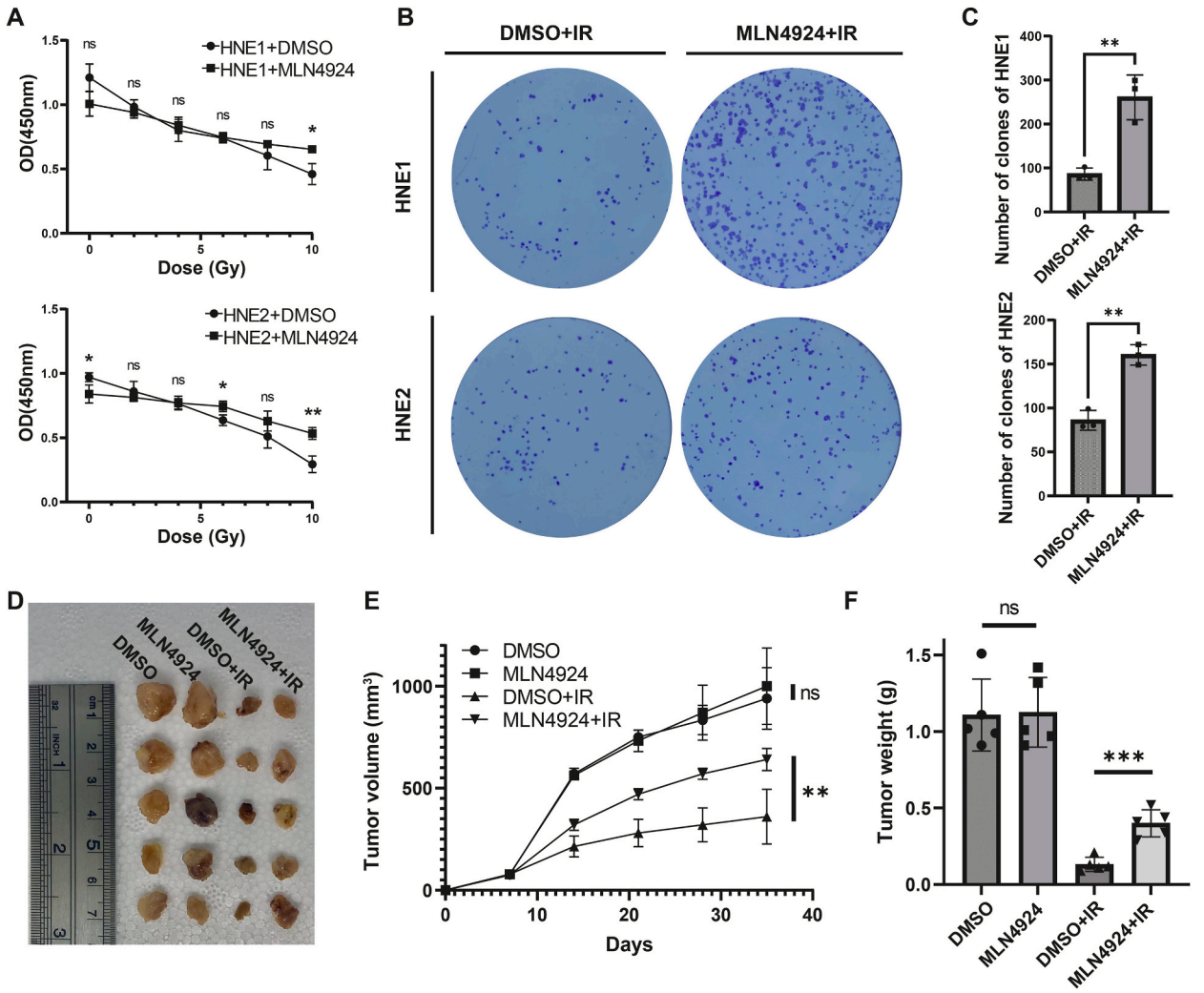

Fig. 3. Impact of MLN4924 treatment on radiotherapy sensitivity of NPC cells. (A) OD values from CCK8 assays of HNE1 and HNE2 cells after different radiation doses, significance: $^{**}P < 0.01$, $^{*}P < 0.05$, $^{ns}P \geq 0.05$. (B) Colony formation assay results of HNE1 and HNE2 cells after radiation. (C) Statistical analysis of colony formation numbers in HNE1 and HNE2 cells after radiation, significance: $^{**}P < 0.01$. (D) Tumor formation assay results of HNE1 cells after radiation. (E) Tumor cell volume at different time points during tumor formation assays with HNE1 cells, significance: $^{**}P < 0.01$, $^{ns}P \geq 0.05$. (F) Statistical analysis of tumor weight in tumor formation assays with HNE1 cells, significance: $^{***}P < 0.001$, $^{ns}P \geq 0.05$.

cytotoxic effect on all cell lines except U251, which displayed significant resistance to MLN4924 (Fig. S6A). After treatment with a low dose of MLN4924 (0.3 μM) combined with 10 Gy of radiotherapy, the results showed that FTC-133 and Hep G2 did not exhibit changes in cell viability post-radiotherapy due to MLN4924 treatment (Fig. S6B). In contrast, U251 developed some resistance to radiation following MLN4924 treatment, but this was not statistically significant (Fig. S6B). However, MLN4924 treatment made MCF7 more sensitive to radiation (Fig. S6B).

3.4. NAE1-associated genes construct prognostic model for NPC

Using single-cell data from NPC epithelial cells, WGCNA analysis determined a soft threshold of 14 based on Scale-free Topology Model Fit >0.8 and the highest average connectivity before network saturation (Fig. S7A). The hierarchical clustering results aligned well with the co-expression modules identified by WGCNA (Fig. S7B). Correlation analysis between module eigengenes (MEs) and NAE1 revealed that the black and darkturquoise modules had the strongest association with NAE1 (Fig. S7C). Enrichment analysis of all genes in the black and darkturquoise modules (Figs. S7D–E) indicated their primary involvement in ribosome assembly and function, post-transcriptional regulation of RNA, and nucleic acid transport (Fig. S7F). Univariate COX regression analysis of genes from these modules in the GSE102349 dataset identified numerous genes impacting patient prognosis (Fig. S7G). The 88 samples from the GSE102349 dataset were randomly divided into a training set (44 samples) and a test set (44 samples). Genes from the black and darkturquoise modules with significant univariate Cox regression results ($P < 0.05$) were included in subsequent modeling (Fig. S7G).

The LASSO penalized Cox regression model identified the most significant PFS predictive genes, constructing the risk score model with the optimal λ value of −2.57 (Fig. 4A). Seven genes were selected to formulate the risk score model (Fig. 4B) with the equation: 0.52424846 × TPI1 + 0.16693444 × PUM1 + 0.08078666 × GAPDH - 0.93422779 × GPX1 - 0.43663713 × ZZZ3 - 0.33762625 × MECOM - 0.19269657 × LINC00869. The risk scores were calculated for the training set, dividing it into high-risk and low-risk groups based on the median. K-M analysis indicated that the low-risk group had better prognosis and fewer progression events compared to the high-risk group (Fig. 4C–D). Similar results were observed in the test set and whole set (Fig. 4C–D). Time-dependent ROC analysis demonstrated excellent and stable PFS predictive capacity of the model across the three sets (Fig. 4E). Retrospective analysis using immunohistochemistry on NAE1-stained sections from 44 primary NPC patients (Fig. 5A) showed that patients with low NAE1 expression had the poorest prognosis (Fig. 5B), although the P-value for three-group survival analysis did not reach significance (P = 0.23). Additionally, qPCR analysis of TPI1, PUM1, GAPDH, GPX1, ZZZ3, MECOM, and LINC00869 mRNA expression in 46 primary NPC samples allowed calculation of risk scores. Retrospective analysis showed that patients with high risk scores had significantly poorer prognosis (Fig. 5C).

4. Discussion

NPC is an Epstein-Barr virus-related cancer originating in the nasopharynx, exhibiting distinctive ethnic and geographic distribution characteristics. Currently, radiotherapy remains the primary treatment for the majority of newly diagnosed NPC cases. Studies indicate that NPC can evade radiation-induced cytotoxicity by altering the expression profile of cell cycle-related genes. This study identifies MLN4924 as a drug targeting NAE1, previously believed to have anti-NPC effects. While demonstrating some anti-tumor efficacy, MLN4924 concurrently induces radioresistance.

NAE1 is essential for cell cycle progression through the S/M checkpoint. Extensive research findings indicate elevated levels of neddylation enzymes and their products in both solid tumor cells and hematologic malignancies, such as lung cancer, liver cancer,

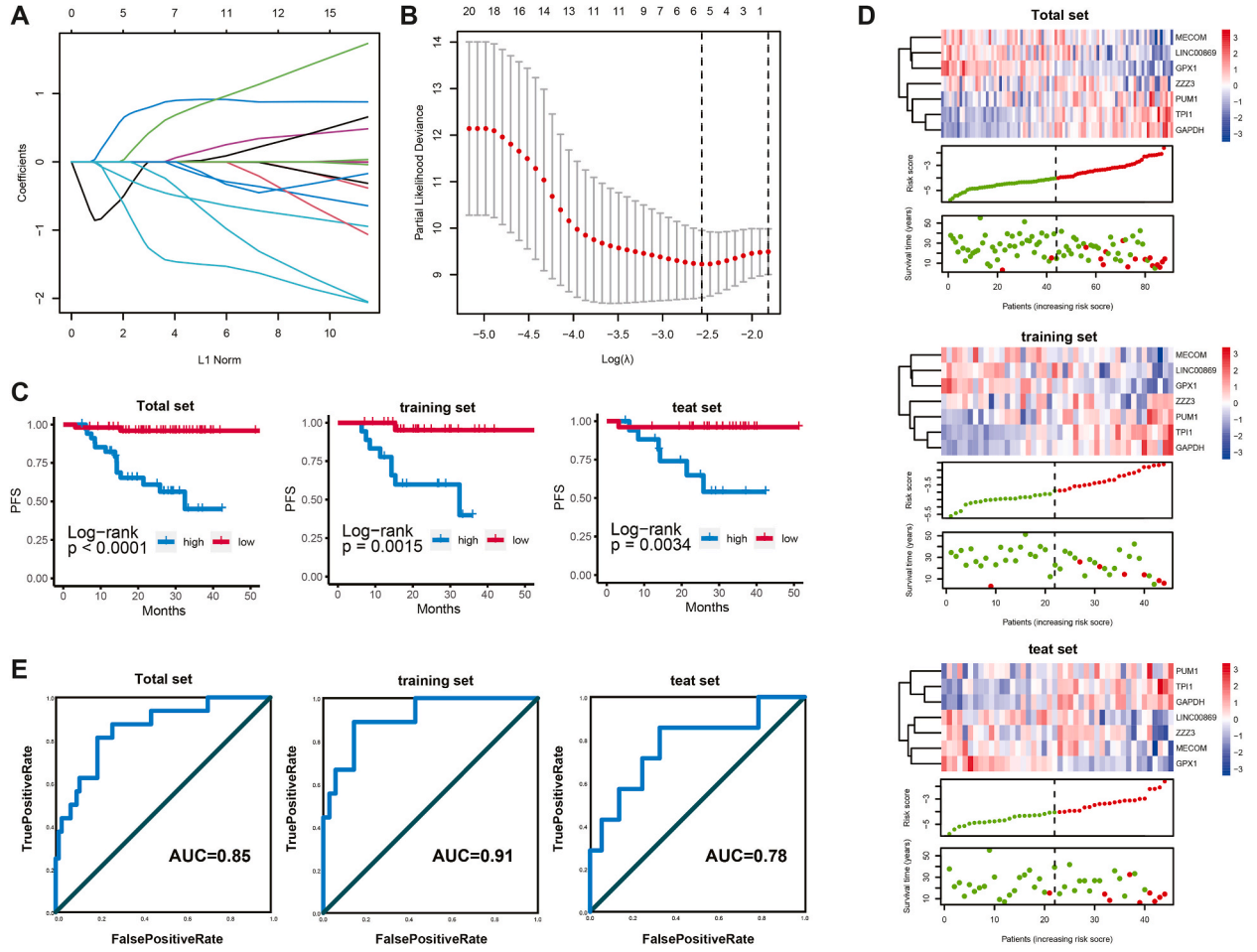

Fig. 4. Construction of NPC prognostic model using NAE1 gene-related gene sets. (A) LASSO regression coefficients. B. LASSO cross-validation. (C) Kaplan-Meier curve for PFS based on risk score. (D) Heatmap of gene expression and patient survival distribution based on risk score model. (E) ROC curves of the LASSO models.

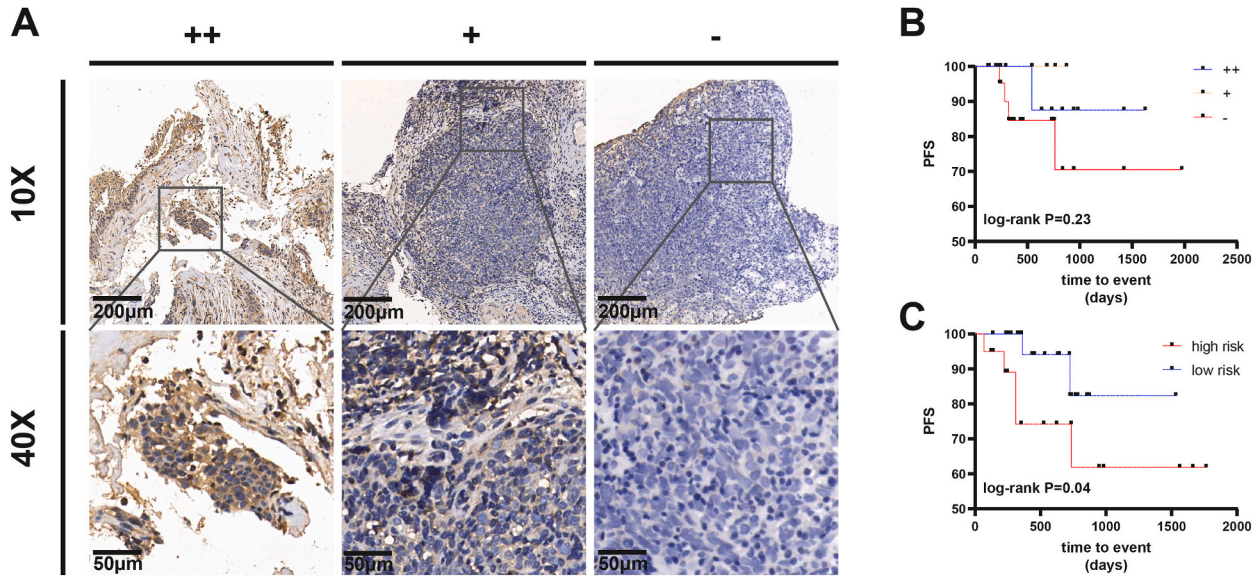

Fig. 5. Validation of NAE1 and NAE1-related gene risk prognostic models in real cohorts. (A) Immunohistochemistry showing expression of NAE1 in primary NPC tissues (n = 44). (B) Kaplan-Meier curve analysis for PFS in NAE1 high, medium, and low expression groups (n = 44). (C) Kaplan-Meier curve for PFS based on risk score in the real cohort (n = 46).

NPC, prostate cancer, and renal cell carcinoma, compared to normal cells. Overactivation of neddylation modification in most tumors correlates with disease progression, significantly reducing overall survival rates for patients [15,16]. As mentioned earlier, hyperactivation of the neddylation modification pathway leads to an overall increase in neddylation modification levels of substrate CRLs (Cullin-RING ligases), thereby promoting the degradation of tumor suppressor genes such as p27 or p21. This process facilitates tumor initiation and progression [17,18]. Given that excessive activation of CRLs contributes to cancer growth and development, targeting neddylation modification could be an attractive approach for cancer therapy [19,20]. MLN4924 has recently been found to be a potent and highly selective small molecule inhibitor of NAE1, blocking protein neddylation modification by inhibiting the first step of the neddylation cascade [7]. In preclinical studies, MLN4924 has demonstrated potent anti-tumor activity and good tolerability. It has progressed into a series of phase I/II/III clinical trials for patients with solid tumors and hematologic malignancies [8–11,21,22].

In NPC, both in the GSE102349 dataset and our own follow-up cohort, we have identified NAE1 as a favorable prognostic factor. This finding may be attributed to the fact that nearly all cases of NPC choose radiotherapy as the primary treatment following diagnosis. NAE1 catalyzes the specific covalent attachment of NEDD8 to substrate proteins, a process known as neddylation modification. Studies have shown that deficiency in the NEDDylation modification system leads to cell cycle arrest at the G2/M phase and contributes to chromosomal aggregation and segregation defects [23]. CRLs represent the classical downstream proteins of NEDD8. Additionally, CRLs constitute the largest family of ubiquitin ligases within cells, functioning to regulate the degradation of various functional proteins [24]. Inhibition of the NEDDylation pathway leads to the accumulation of various substrates of CRLs, as they cannot undergo ubiquitination and subsequent degradation. Examples include CDT1, CDK inhibitors like p21 and p27 [25], and the checkpoint kinase Wee1 [5]. This accumulation results in cell cycle arrest at the G2/M phase, leading to apoptosis or senescence [6]. The relationship between the cell cycle and radioresistance is closely intertwined. Radiotherapy functions by damaging the DNA of cancer cells, thereby preventing their division and growth. Based on the molecular mechanisms through which NAE1 exerts its effects, we have conducted an analysis of the possible reasons for NAE1-mediated radiotherapy resistance in NPC: 1) NEDDylation is crucial for the functional regulation of DNA damage repair proteins [26]. For instance, NEDDylation activates the CUL4A-DDB1 complex, which is a ubiquitin E3 ligase complex. This complex may inhibit the nucleotide excision repair (NER) pathway by ubiquitinating and degrading key proteins involved in NER, thereby affecting DNA damage repair [27]. Additionally, NEDDylation can influence the choice between homologous recombination repair (HRR) and non-homologous end joining (NHEJ) pathways by modifying and regulating critical repair proteins such as 53BP1, thus inhibiting high-fidelity DNA damage repair [28]. The regulation of DNA damage repair genes by NEDDylation is complex and multifaceted, warranting further investigation. 2) According to our research findings, NAE1 has a significant impact on the cell cycle progression of NPC. Therefore, the influence of the cell cycle on radiotherapy sensitivity may play a more substantial role in NAE1-targeted treatment of NPC. When NEDDylation is inhibited, G2/M phase genes, including CDT1, p21, and p27, accumulate, causing NPC cells to enter and arrest in the G2/M phase, which is relatively insensitive to radiation [29]. However, our study only demonstrates the phenomenon that inhibiting NAE1 alters the sensitivity of NPC to radiation; the specific molecular mechanisms underlying this change require further investigation.

In a study on NPC, contrary to our findings, researchers demonstrated through immunohistochemical staining of 197 NPC tissues that elevated NEDD8 expression is an unfavorable independent factor for overall survival and disease-free survival [15]. In our study, specific inhibition with MLN4924 significantly suppressed NPC cell proliferation, induced apoptosis, and caused cell cycle arrest.

However, our findings from two independent cohorts indicate that high NAE1 expression can serve as a favorable prognostic factor. Therefore, we believe the potential clinical application of MLN4924 in NPC warrants further investigation. Several reasons may explain the contradictory findings between the two studies: 1) The relationship between NAE1 expression and prognosis may be influenced by treatment modalities; 2) The timing and dosage of MLN4924 administration could impact its ability to directly inhibit cell proliferation or induce changes in gene expression during the G2/M phase, potentially leading to radiotherapy resistance; 3) Moreover, exploring whether NAE1 has alternative pathways independent of neddylation involved in NPC radioresistance merits deeper investigation.

Ethics statements

The studies involving human participants were reviewed and approved by Ethics Committee of Qingdao Municipal Hospital (Approval No: 2024-KY-032). The patients/participants provided their written informed consent to participate in this study. Written informed consent was obtained from the individual(s) for the publication of any potentially identifiable images or data included in this article. Animal experiments were approved by the Ethics Committee of Qingdao Municipal Hospital (Approval No.: 2024-KY-032).

Consent for publication

All information was collected with the consent of the patient and approved by our institutional ethics department.

Data availability

Data will be made available on request.

Funding information

This research was funded by the Qingdao Medical and Health Research Guidance Program (2023-WJZD178).

CRediT authorship contribution statement

Qinsong Liu: Methodology, Investigation. **Lu Xin:** Data curation. **Xiaoning Ma:** Validation. **Yong Yuan:** Project administration, Conceptualization.

Declaration of competing interest

The authors declare that they have no known competing financial interests or personal relationships that could have appeared to influence the work reported in this paper.

Acknowledgements

Not applicable.

Appendix A. Supplementary data

Supplementary data to this article can be found online at https://doi.org/10.1016/j.heliyon.2024.e37219.

References

[1] Y.P. Chen, A.T.C. Chan, Q.T. Le, P. Blanchard, Y. Sun, J. Ma, Nasopharyngeal carcinoma, Lancet Lond Engl 394 (10192) (2019) 64–80, https://doi.org/10.1016/S0140-6736(19)30956-0.
[2] A.W.M. Lee, W.T. Ng, J.Y.W. Chan, J. Corry, A. Mäkitie, W.M. Mendenhall, et al., Management of locally recurrent nasopharyngeal carcinoma, Cancer Treat Rev. 79 (2019) 101890, https://doi.org/10.1016/j.ctrv.2019.101890.
[3] P. Bossi, A.T. Chan, L. Licitra, A. Trama, E. Orlandi, E.P. Hui, et al., Nasopharyngeal carcinoma: ESMO-EURACAN Clinical Practice Guidelines for diagnosis, treatment and follow-up, Ann Oncol Off J Eur Soc Med Oncol. 32 (4) (2021) 452–465, https://doi.org/10.1016/j.annonc.2020.12.007.
[4] M. Oladghaffari, J.P. Islamian, B. Baradaran, A.S. Monfared, MLN4924 therapy as a novel approach in cancer treatment modalities, J Chemother Florence Italy 28 (2) (2016) 74–82, https://doi.org/10.1179/1973947815Y.0000000066.
[5] S.Y. Wang, X. Liu, Y. Liu, H.Y. Zhang, Y.B. Zhang, C. Liu, et al., Review of NEDDylation inhibition activity detection methods, Bioorg. Med. Chem. 29 (2021) 115875, https://doi.org/10.1016/j.bmc.2020.115875.
[6] Y. Zhang, C.C. Shi, H.P. Zhang, G.Q. Li, S.S. Li, MLN4924 suppresses neddylation and induces cell cycle arrest, senescence, and apoptosis in human osteosarcoma, Oncotarget 7 (29) (2016) 45263–45274, https://doi.org/10.18632/oncotarget.9481.
[7] T.A. Soucy, P.G. Smith, M.A. Milhollen, A.J. Berger, J.M. Gavin, S. Adhikari, et al., An inhibitor of NEDD8-activating enzyme as a new approach to treat cancer, Nature 458 (7239) (2009) 732–736, https://doi.org/10.1038/nature07884.

[8] A.N. Saliba, S.H. Kaufmann, E.M. Stein, P.A. Patel, M.R. Baer, W. Stock, et al., Pevonedistat with azacitidine in older patients with TP53-mutated AML: a phase 2 study with laboratory correlates, Blood Adv 7 (11) (2023) 2360–2363, https://doi.org/10.1182/bloodadvances.2022008625.
[9] N.J. Short, M. Muftuoglu, F. Ong, L. Nasr, W. Macaron, G. Montalban-Bravo, et al., A phase 1/2 study of azacitidine, venetoclax and pevonedistat in newly diagnosed secondary AML and in MDS or CMML after failure of hypomethylating agents, J Hematol OncolJ Hematol Oncol. 16 (1) (2023) 73, https://doi.org/10.1186/s13045-023-01476-8.
[10] X. Zhou, D.L. Richardson, A. Dowlati, S. Goel, S. Sahebjam, J. Strauss, et al., Effect of pevonedistat, an investigational NEDD8-activating enzyme inhibitor, on the QTc interval in patients with advanced solid tumors, Clin Pharmacol Drug Dev 12 (3) (2023) 257–266, https://doi.org/10.1002/cpdd.1194.
[11] H. Shoji, D. Takahari, H. Hara, K. Nagashima, J. Adachi, N. Boku, A Phase I study of pevonedistat plus capecitabine plus oxaliplatin in patients with advanced gastric cancer refractory to platinum (NCCH-1811), Future Sci OA 7 (7) (2021) FSO721, https://doi.org/10.2144/fsoa-2021-0023.
[12] A.M. Buckley, N. Lynam-Lennon, H. O'Neill, J. O'Sullivan, Targeting hallmarks of cancer to enhance radiosensitivity in gastrointestinal cancers, Nat. Rev. Gastroenterol. Hepatol. 17 (5) (2020) 298–313, https://doi.org/10.1038/s41575-019-0247-2.
[13] A.J. McIlwrath, P.A. Vasey, G.M. Ross, R. Brown, Cell cycle arrests and radiosensitivity of human tumor cell lines: dependence on wild-type p53 for radiosensitivity, Cancer Res. 54 (14) (1994) 3718–3722.
[14] T.M. Pawlik, K. Keyomarsi, Role of cell cycle in mediating sensitivity to radiotherapy, Int. J. Radiat. Oncol. Biol. Phys. 59 (4) (2004) 928–942, https://doi.org/10.1016/j.ijrobp.2004.03.005.
[15] P. Xie, J.P. Yang, Y. Cao, L.X. Peng, L.S. Zheng, R. Sun, et al., Promoting tumorigenesis in nasopharyngeal carcinoma, NEDD8 serves as a potential theranostic target, Cell Death Dis. 8 (6) (2017) e2834, https://doi.org/10.1038/cddis.2017.195.
[16] P. Xie, M. Zhang, S. He, K. Lu, Y. Chen, G. Xing, et al., The covalent modifier Nedd8 is critical for the activation of Smurf1 ubiquitin ligase in tumorigenesis, Nat. Commun. 5 (2014) 3733, https://doi.org/10.1038/ncomms4733.
[17] L. Zhou, W. Zhang, Y. Sun, L. Jia, Protein neddylation and its alterations in human cancers for targeted therapy, Cell. Signal. 44 (2018) 92–102, https://doi.org/10.1016/j.cellsig.2018.01.009.
[18] Y. Zhao, M.A. Morgan, Y. Sun, Targeting Neddylation pathways to inactivate cullin-RING ligases for anticancer therapy, Antioxidants Redox Signal. 21 (17) (2014) 2383–2400, https://doi.org/10.1089/ars.2013.5795.
[19] L. Jia, Y. Sun, SCF E3 ubiquitin ligases as anticancer targets, Curr. Cancer Drug Targets 11 (3) (2011) 347–356.
[20] Y. Zhao, Y. Sun, Cullin-RING ligases as attractive anti-cancer targets, Curr. Pharmaceut. Des. 19 (18) (2013) 3215–3225.
[21] M.A. Milhollen, T. Traore, J. Adams-Duffy, M.P. Thomas, A.J. Berger, L. Dang, et al., MLN4924, a NEDD8-activating enzyme inhibitor, is active in diffuse large B-cell lymphoma models: rationale for treatment of NF-{kappa}B-dependent lymphoma, Blood 116 (9) (2010) 1515–1523, https://doi.org/10.1182/blood-2010-03-272567.
[22] T.A. Soucy, P.G. Smith, M. Rolfe, Targeting NEDD8-activated cullin-RING ligases for the treatment of cancer, Clin Cancer Res Off J Am Assoc Cancer Res. 15 (12) (2009) 3912–3916, https://doi.org/10.1158/1078-0432.CCR-09-0343.
[23] Z. Li, Q. Cui, X. Wang, B. Li, D. Zhao, Q. Xia, et al., Functions and substrates of NEDDylation during cell cycle in the silkworm, Bombyx mori, Insect Biochem. Mol. Biol. 90 (2017) 101–112, https://doi.org/10.1016/j.ibmb.2017.09.013.
[24] K. Tateishi, M. Omata, K. Tanaka, T. Chiba, The NEDD8 system is essential for cell cycle progression and morphogenetic pathway in mice, J. Cell Biol. 155 (4) (2001) 571–580, https://doi.org/10.1083/jcb.200104035.
[25] A.S. Kittai, O.V. Danilova, V. Lam, T. Liu, N. Bruss, S. Best, et al., NEDD8-activating enzyme inhibition induces cell cycle arrest and anaphase catastrophe in malignant T-cells, Oncotarget 12 (20) (2021) 2068–2074, https://doi.org/10.18632/oncotarget.28063.
[26] N.A. Wilkinson, K.S. Mnuskin, N.W. Ashton, R. Woodgate, Ubiquitin and ubiquitin-like proteins are essential regulators of DNA damage bypass, Cancers 12 (10) (2020) 2848, https://doi.org/10.3390/cancers12102848.
[27] M. Meyers, S. Cismoski, A. Panidapu, B. Chie-Leon, D.K. Nomura, Targeted protein degradation through recruitment of the CUL4 complex adaptor protein DDB1, ACS Chem. Biol. 19 (1) (2024) 58–68, https://doi.org/10.1021/acschembio.3c00487.
[28] A. Schellenbauer, M.N. Guilly, R. Grall, R. Le Bars, V. Paget, T. Kortulewski, et al., Phospho-Ku70 induced by DNA damage interacts with RNA Pol II and promotes the formation of phospho-53BP1 foci to ensure optimal cNHEJ, Nucleic Acids Res. 49 (20) (2021) 11728–11745, https://doi.org/10.1093/nar/gkab980.
[29] Y. Wang, S. Oda, M.G. Suzuki, H. Mitani, F. Aoki, Cell cycle-dependent radiosensitivity in mouse zygotes, DNA Repair 117 (2022) 103370, https://doi.org/10.1016/j.dnarep.2022.103370.